

Coverage Dependent Evolution of Two-Dimensional Dendrimer/Mica Domain Patterns

F. T. Xu,[†] S. C. Street,[‡] and J. A. Barnard^{*,†}

Department of Materials Science and Engineering, University of Pittsburgh, Pittsburgh, Pennsylvania 15261,
and Center for Materials for Information Technology, The University of Alabama,
Tuscaloosa, Alabama 35487-0209

Received: May 20, 2003; In Final Form: September 16, 2003

For a two-dimensional, two-phase system of A and B, with competing short-range attractive and long-range repulsive interactions, the evolution of domain patterns as a function of area fraction should follow the sequence circular islands of A in a matrix of B (the droplet phase), alternating elongated domains of A and B (the striped phase), and circular islands of B in a matrix of A (the inverted droplet phase). The predicted domain pattern evolution is experimentally verified here for the case of dendrimer molecules on mica, a materials system amenable to control of the competing interactions. This result, along with the coverage dependence of the characteristic domain length scale, is reported for the first time. The domain patterns are fabricated by simple aerosol deposition of dilute solutions of dendrimer molecules in pentanol onto mica followed by slow evaporation. The long-range repulsive interaction in this case is electrostatic in origin and is associated with the contact potential between the negatively charged surface of mica submerged in pentanol and the positively charged surface of the dendrimer molecule domains.

1. Introduction

The formation of stable, two-dimensional (2D), two-phase domain patterns resulting from competing short-range attractive and long-range repulsive interactions has been explored theoretically^{1–5} and observed experimentally^{6–13} in a number of quite different materials systems. The short-range attractive interaction is always associated with minimization of interphase boundary length while the long-range repulsive interaction is attributed, for example, to electrostatic, magnetic, and elastic interactions, depending on the physics of the system. For systems with domain sizes much larger than the domain boundary width, the characteristic domain length scale, l_0 , at thermodynamic equilibrium is given by⁴

$$l_0 = \pi a \exp(\gamma_b/\gamma_d + 1) \quad (1)$$

where γ_b is an energy per unit length of the interphase boundary, γ_d is proportional to the square of the difference in the “dipole density” between the two phases, and a is a length quantifying the sharpness of the interphase interface. In the simplest cases γ_b can be assumed to be isotropic. The appropriate dipole density in each phase depends on the physical situation (the screened electric dipole density normal to the water/air interface is used for Langmuir layers while surface stress is invoked for overlayer structures on surface alloys). The opportunity to control l_0 and thus pattern formation at the nanoscale over large areas by controlling the γ_b/γ_d ratio has exciting technological implications.

For a two-phase system of A and B, and competing interactions as described above, the evolution of domain patterns as a function of the area fraction, $f = f_A = 1 - f_B$, has been predicted⁴ to follow the sequence circular islands of A in a matrix of B (the droplet phase), alternating elongated domains

of A and B (the striped phase), and circular islands of B in a matrix of A (the inverted droplet phase). The degree of long-range order and the uniformity of domain sizes and shapes actually observed depend on both the thermal noise present and the proximity to equilibrium. This very basic prediction of pattern evolution has only very recently been experimentally confirmed¹³ for the first time for incommensurate Pb overlayers grown on a Pb/Cu surface alloy prepared under ultrahigh vacuum conditions and imaged by low-energy electron microscopy. Surface stress differences between the overlayer and alloy structures are the origin of γ_d in this case. In the following we demonstrate that the predicted domain pattern evolution is also found in a completely different materials system consisting of dendrimer molecules adsorbed onto the surface of freshly cleaved mica. In our case the domain patterns are fabricated by simple aerosol deposition of dilute solutions of dendrimer molecules in pentanol under ambient conditions followed by slow evaporation. γ_d is expected to be electrostatic in origin in this case and is associated with the contact potential between the negatively charged surface of mica submerged in pentanol and the positively charged surface of the dendrimer molecule domains.

Dendrimers are three-dimensional, globular, highly branched macromolecules made up of a focal point core surrounded by repeated branch units all enclosed by a terminal group “shell”. They can be synthesized with highly controllable sizes (they are essentially monodisperse) determined by the core type, extent of branching, and nature of the end groups, in the range from a few to several tens of nanometers in diameter.^{14–17} They have received intensive interest associated with their variable size, the controllable chemistry of their surfaces, and their potential for serving as the host for metal (and other) nanoparticles.^{18–20} Dendrimers can also readily form flat, complete monolayers on technologically interesting substrates using standard cleaning, dipping, and rinsing procedures.^{21–23} Dendrimer monolayers are receiving increasing attention with regard to their adhesive,

* Corresponding author. E-mail: jbarnard@engr.pitt.edu.

[†] University of Pittsburgh.

[‡] The University of Alabama.

frictional, and tribological behavior as well as for their potential in mediating the growth mode and quality of ultrathin metal films.^{21,24–27} By contrast, the self-organized growth of complex submonolayer dendrimer patterns observed when finite volumes of dendrimer solution are cast on a substrate in a thin layer and allowed to evaporate^{28–30} has received comparatively little attention.

The basic physical picture envisaged for dendrimer layer growth by immersion (dipping) of a suitable substrate into a dendrimer-containing solution is that isolated dendrimer molecules dispersed in an appropriate solution randomly adsorb on the substrate surface and stick with some (unknown) probability. Dendrimer molecules progressively fill up the surface, forming a close-packed monolayer. Simultaneous or subsequent multilayer formation also may occur. Careful rinsing of films fabricated in this way removes the more loosely bound dendrimers (those not in direct contact with the substrate), leaving behind a flat and uniform monolayer. The situation is very different for thin cast films where the reservoir of dendrimer molecules is finite, dendrimer attachment at the substrate occurs during evaporation, and the dendrimer structures which form are eventually subject to the forces of dewetting. Dewetting^{31–35} occurs via nucleation of holes or dry patches as the fluid film thickness decreases due to evaporation. Once nucleated, holes grow and ultimately impinge to produce contact lines forming a cellular structure. For the case of an evaporating dendrimer solution the extent to which the forces associated with dewetting influence the final dried dendrimer structure will depend on the strength of the dendrimer molecule/substrate interaction and the relative time scales for dendrimer domain formation and fluid film thinning. Little is known quantitatively about dendrimer mobility at the substrate/dendrimer solution interface. Significant lateral diffusion in the presence of a solvent, if not desorption/readsorption, is generally assumed and is necessary in accounting for many dendrimer film structures, including those described below.

It is well established that poly(amidoamine) (PAMAM) dendrimers, which are roughly spherical in solution, “collapse” when adsorbed onto substrate surfaces. Heights (thicknesses) of both isolated molecules and monolayers (measured by scanning probe microscopy, SPM, and X-ray reflectivity, XRR) are typically something less than half the diameter in solution, independent of generation. This is true not only of dried structures but also of adsorbed isolated dendrimers measured *in situ* at the liquid/substrate interface.³⁶ For example, generation 4 (G4) PAMAM dendrimers, with a solution diameter of ~ 4.5 nm, display monolayer thicknesses on silicon ranging from 1.1 to 1.7 nm (SPM) and from 1.4 to 2.2 nm (XRR).^{14,37–39}

2. Experimental Section

Dendrimer film structures were prepared by aerosol deposition using an EFFA Spray Mounter MK II (Ernest F. Fullam, Inc.). Aerosol deposition is a convenient way to rapidly and relatively uniformly transport a finite volume of fluid to a substrate to form a thin fluid layer. Droplet diameters in the aerosol ranged from 20 to 40 μm . Droplets coalesced on arrival at the substrate, forming a continuous fluid film. The average droplet diameter is at least an order of magnitude larger than the dendrimer domain sizes and spacings observed by AFM of the subsequently dried adsorbed dendrimer patterns, convincing evidence that the droplets are not determining pattern formation which extends over hundreds of micrometers. All structures were produced by aerosol deposition and subsequent evaporation of 0.05 weight percent (wt %) pentanolic solutions of generation

4 (G4) PAMAM-25% C₁₂ dendrimers (48 primary amino surface groups and 16 *N*-(2-hydroxydodecyl) surface groups; theoretical molecular weight 20 113 amu) obtained as a 10 wt % methanolic solution from Aldrich (Milwaukee, WI). This modified G4 PAMAM dendrimer, hereafter G4-25%C₁₂, has not to our knowledge been studied in the open literature. It was selected because the *N*-(2-hydroxydodecyl) chains which replace 25% of the terminal amine groups found in a standard G4 PAMAM dendrimer were expected to enhance the dendrimer molecule/substrate interaction, leading to stronger adhesion while maintaining surface mobility sufficient to allow the system to approach equilibrium. Dynamic light scattering has been used to determine a hydrodynamic diameter of ~ 10.7 nm for G4-25%C₁₂ as received in methanolic solution. On the basis of the general tendencies noted above, a G4-25%C₁₂ monolayer (ML) adsorbed on a substrate would be expected to have a height of 4–5 nm. The pentanolic solutions were prepared by simple volumetric dilution using pipets with disposable tips from fresh commercial methanol-based solutions. The extremely uniform thickness (1 ML) and flatness of the dendrimer film structures discussed below are consistent with dendrimers dispersed at the molecular level, both in the aerosol droplet and following coalescence on the substrate, and not agglomerated into various sized assemblies prior to deposition. The total volume of fluid used and the substrate area coated yielded a continuous fluid film ~ 15 μm thick (neglecting evaporation in flight) on a substrate of freshly cleaved mica. The pentanolic fluid film evaporated slowly (~ 10 min). Evaporation does cause “pooling” of fluid ahead of growing dry patches, leading to variations in the size of the reservoir of dendrimer molecules available to form film structures. This accounts for the variation observed in film structure at the scale of hundreds of micrometers. The dried dendrimer surface structures were characterized by atomic force microscopy (AFM) in “tapping mode” with a standard tip (Digital Instruments, Inc., model D-3100). Freshly cleaved bare mica surfaces exhibit rms roughness of 0.085 nm, while the roughness at the free surface of the dendrimer domains is just slightly higher, 0.124 nm. All images shown are representative of regions extending several hundred microns or more. The patterns shown are stable under ambient conditions over many weeks.

3. Results and Discussion

This section discusses systematically the evolution of dendrimer domain structure and morphology as a function of area fraction (or “coverage”) of the mica substrate covered by dendrimer molecules, *f*. As will become apparent, all of the dendrimer domains have essentially the same thickness (~ 4.7 nm) independent of *f*, which corresponds well to the 1 ML thickness expected for G4-25%C₁₂. The structures discussed below are purely 2D with no evidence for formation of a partial second or subsequent dendrimer layer. Under these conditions this is an experimental realization of a 2D, two-phase system with 1 ML thick dendrimer domains and bare mica serving as the two phases. The dark contrast in the images is the mica substrate. For clarity, all images shown are 5 $\mu\text{m} \times 5 \mu\text{m}$, but the quantitative image analysis reported is based on a 10 $\mu\text{m} \times 10 \mu\text{m}$ region which encompasses the displayed area.

At the lowest coverages studied (*f* = 0.13; Figure 1a) the dendrimers are organized into dispersed, primarily circular domains (islands) of varying diameters. Some of the domains are extended in form, and these linear shapes are consistent with coalescence of neighboring circular domains. All of the dendrimer domains have rounded perimeters. At this coverage, the

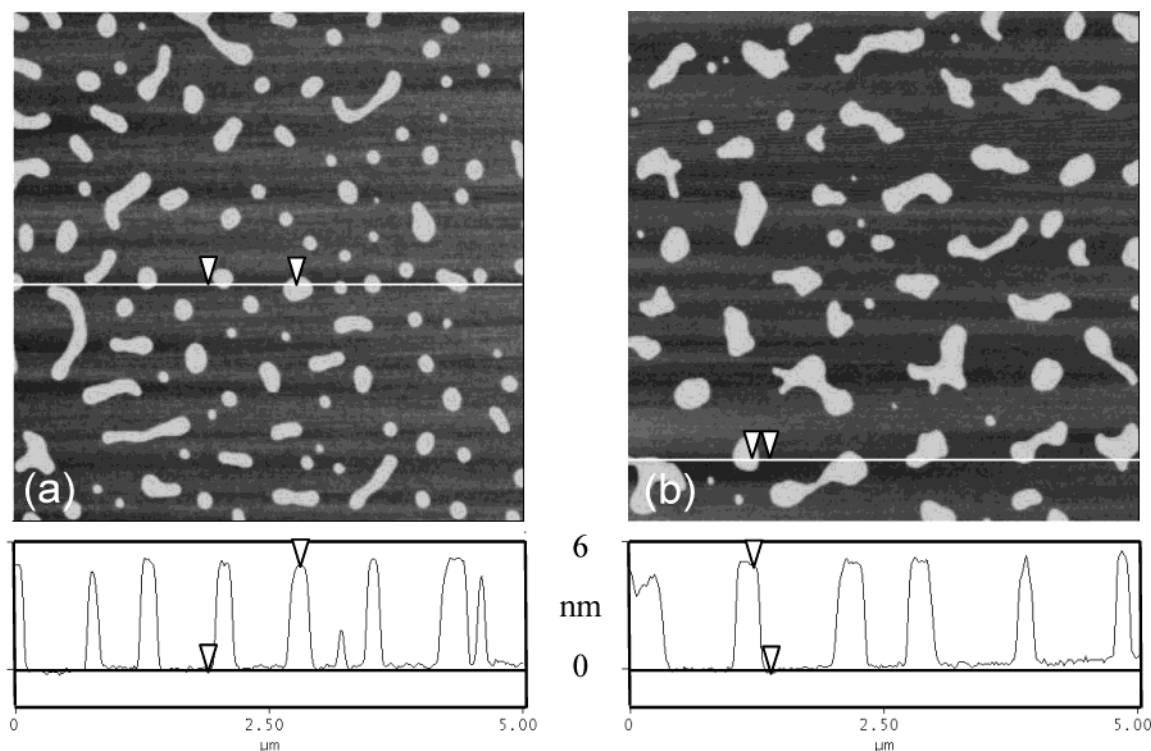


Figure 1. Representative plan-view AFM images ($5\ \mu\text{m} \times 5\ \mu\text{m}$) and cross sections of domain structures formed by aerosol deposition of G4 PAMAM-25% C_{12} dendrimer solution on mica: (a) $f = 0.13$; (b) $f = 0.16$.

mean domain size expressed as the diameter (d) of the equivalent circle calculated from the mean area of the domains is ~ 190 nm. Domains of this size contain hundreds of individual dendrimer molecules, although no internal contrast is apparent. A topographic profile along a line selected to pass through a number of domains reveals the fact that the domains have a very consistent height, h , in this case averaging 4.76 nm. The only height deviations observed are when the section line cuts close to the edge of a domain where the finite size of the AFM tip introduces a nonphysical slope from the top of the domain down to the mica surface. Increasing the coverage to $f = 0.16$ (Figure 1b) leads to similarly dispersed domains with a greater preponderance of larger elongated shapes. The mean domain diameter as defined above is ~ 250 nm. The cross section again confirms that the domains have a single height (in this case averaging 4.74 nm).

It is also useful to quantify the perimeter, P , and area, A , of the domains in Figure 1a and plot them as shown in Figure 2. The slope of the P versus A plot has been used to suggest plausible mechanisms of microstructural evolution.⁴⁰ For the smallest domains, each domain is roughly circular and, thus, $P \propto A^{1/2}$, as observed. The microstructure which evolves at or very near equilibrium as the coverage changes should be independent of the mechanism by which molecular rearrangements may occur. Nevertheless, a possible mechanism for formation of the larger, elongated domains consistent with both the appearance of the domains and the clearly observed $P \propto A$ dependence is that these ramified domains could have formed by development of a “neck” between neighboring, smaller, more circular domains. The coexistence of ramified and compact domains in certain coverage ranges was also observed in the Pb overlayer system,¹³ and island migration was proposed as the mechanism responsible for microstructural evolution.

As the coverage is further increased to $f = 0.23$ (Figure 3a), several important features are noted. Most of the domains are elongated but not necessarily along a single direction.

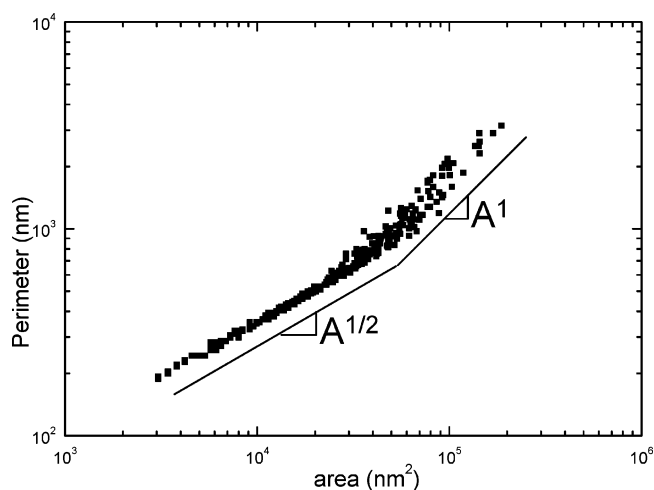


Figure 2. Perimeter, P , versus area, A , of the dendrimer domains in Figure 1a.

Variations in domain width along the length are noted, and very interestingly, many domains contain circular “holes” which penetrate all the way to the mica surface. The domains are significantly larger ($d \sim 310$ nm), and the cross section yields a domain height of $h = 4.63$ nm. At $f = 0.33$ (Figure 3b), somewhat smaller ($d \sim 270$ nm), elongated domains creating a labyrinthine structure dominate although some small rounded domains still remain. The holes noted at $f = 0.23$ are even more prevalent. The dendrimers continue to organize themselves into 1 ML thick structures with $h = 4.70$ nm at this coverage. The dendrimer domains are clearly nearing their 2D percolation threshold.

At $f = 0.39$ (Figure 4a) percolation is reached and the resulting structure can be seen as two interpenetrating contiguous phases, the 1 ML thick dendrimer domains ($h = 4.72$ nm) and the bare mica surface. At all higher coverages the system is inverted with the dendrimer monolayer regions now the “matrix”

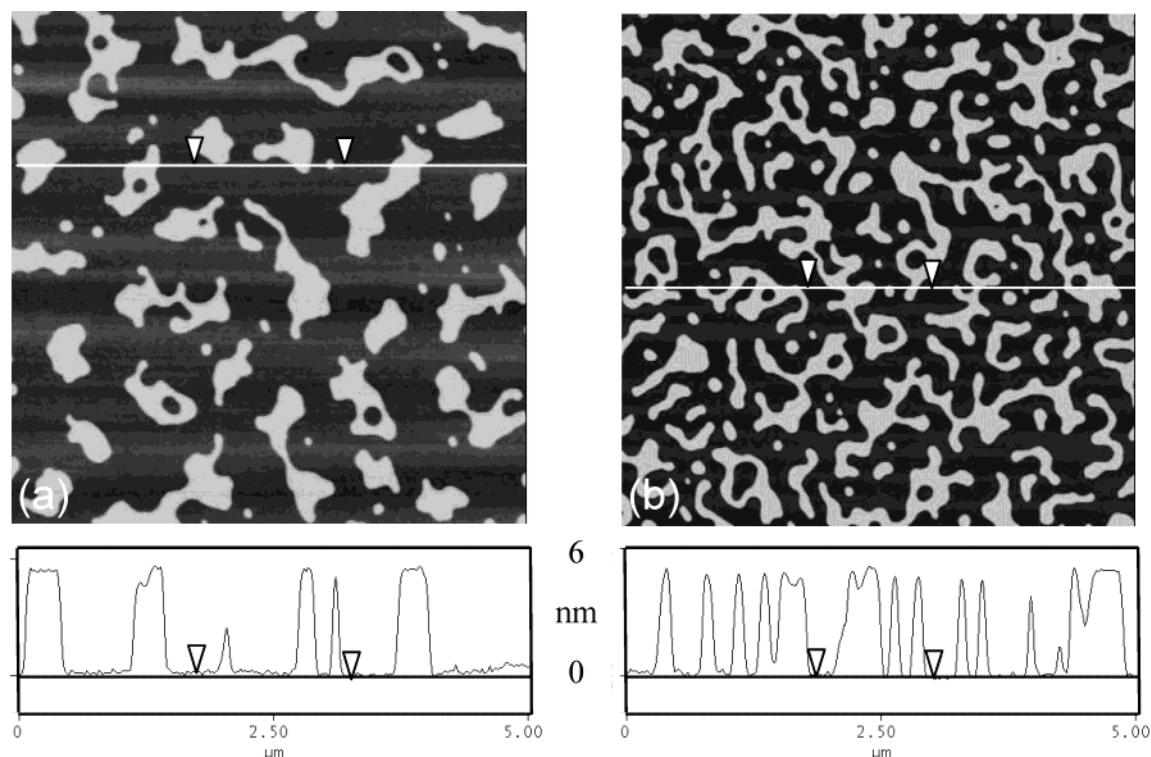


Figure 3. Representative plan-view AFM images ($5\ \mu\text{m} \times 5\ \mu\text{m}$) and cross sections of domain structures formed by aerosol deposition of G4 PAMAM-25% C_{12} dendrimer solution on mica: (a) $f = 0.23$; (b) $f = 0.33$.

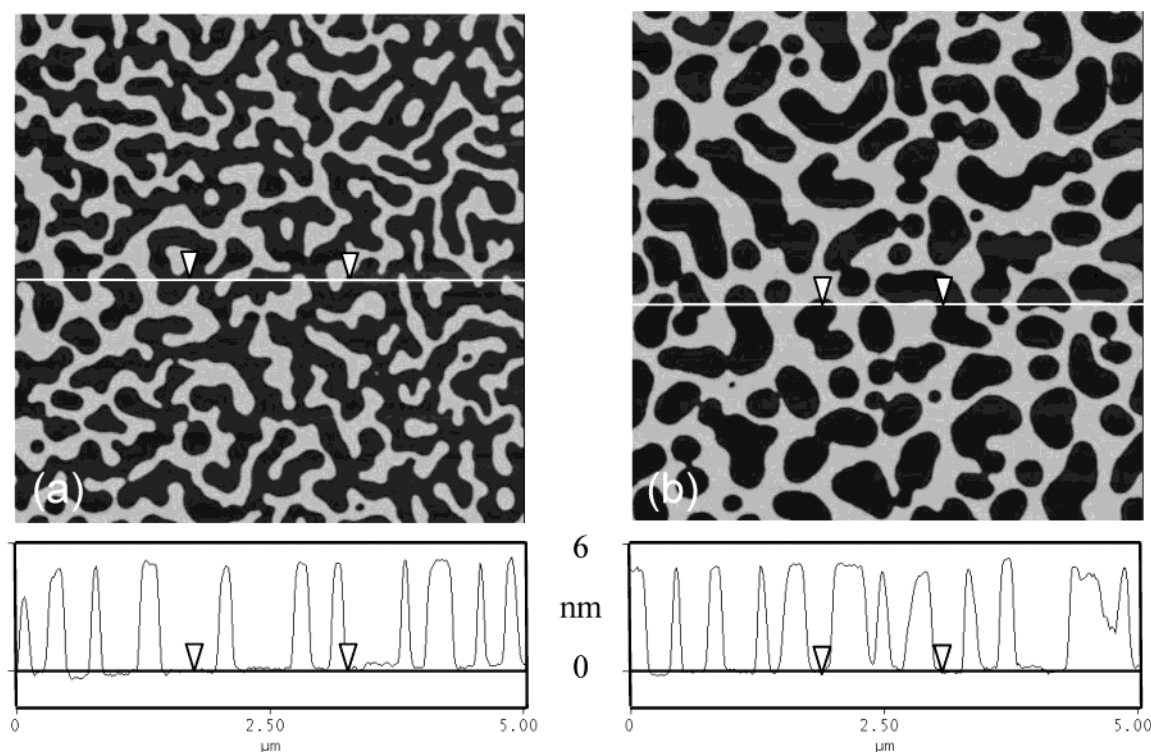


Figure 4. Representative plan-view AFM images ($5\ \mu\text{m} \times 5\ \mu\text{m}$) and cross sections of domain structures formed by aerosol deposition of G4 PAMAM-25% C_{12} dendrimer solution on mica: (a) $f = 0.39$; (b) $f = 0.45$.

in the two-phase system. At $f = 0.45$ (Figure 4b) the bare mica patches assume primarily elongated forms with rounded edges. The thickness of the dendrimer monolayer remains consistent through the inversion ($h = 4.71\ \text{nm}$ at this coverage). As f continues to increase (Figure 5; $f = 0.52$ and $f = 0.64$; $h = 4.70$ and $h = 4.77$), the bare mica patches become smaller and more circular, tracking, in reverse sequence, the evolution observed in the dendrimer domains at low coverage (Figure 1).

In this coverage range the bare mica surface is the “inverted droplet” phase. Perimeter versus area analysis of the bare mica patches, as illustrated in Figure 2 for the dendrimer domains, yields the same transition in behavior from $P \propto A$ to $P \propto A^{1/2}$ as the patches become smaller (not shown). At higher coverages ($f > 0.7$; not shown) the mica patches continue to decrease in size and nearly all are roughly circular (very few elongated forms).

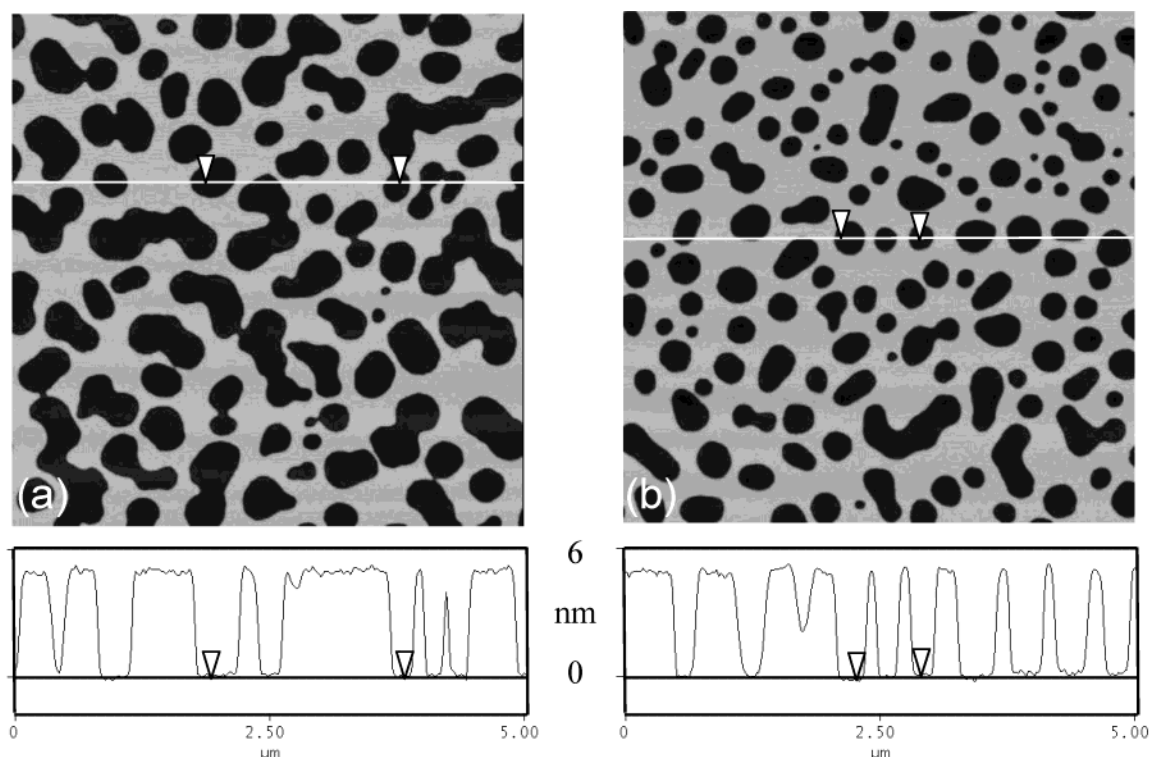


Figure 5. Representative plan-view AFM images ($5\ \mu\text{m} \times 5\ \mu\text{m}$) and cross sections of domain structures formed by aerosol deposition of G4 PAMAM-25% C_{12} dendrimer solution on mica: (a) $f = 0.52$; (b) $f = 0.64$.

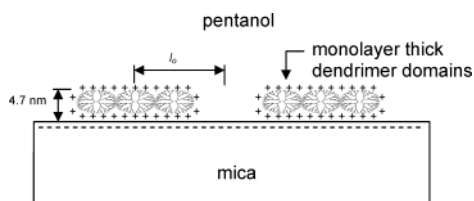


Figure 6. Schematic illustration of the expected charge state of the mica surface and dendrimer domains during growth of the 2D dendrimer domains.

Figures 1 and 3–5 clearly demonstrate the predicted droplet–stripe–inverted stripe sequence, albeit with a considerable amount of disorder. Figure 6 schematically illustrates the expected charge state of the mica surface and dendrimer domains which we propose as the origin of the long-range repulsive interaction necessary to stabilize the observed sequence. The mica surface (which when freshly cleaved is covered with K^+ ions) is expected to exhibit a negative charge due to loss of K^+ ions from the mica surface into the pentanol. This surface dissolution and resulting surface charging has been invoked in surface force balance measurements of the interaction between mica surfaces submerged in water.⁴¹ Our assumption is that a negatively charged mica surface is present during the growth of the 2D dendrimer domains. The dendrimer molecules themselves and the domains they form have a positive surface charge due to protonation of their terminal amine groups. Such positively charged G4 PAMAM dendrimers have been used as one component in electrostatic layer-by-layer deposition of multilayers of oppositely charged dendrimers.³⁹ In our case, mobile, positively charged dendrimers organize themselves into the observed domain patterns while submerged in pentanol. The dendrimer patterns which form are highly stable and are preserved during evaporation, showing no evidence of the cellular structures which can result from the forces of dewetting.³⁰

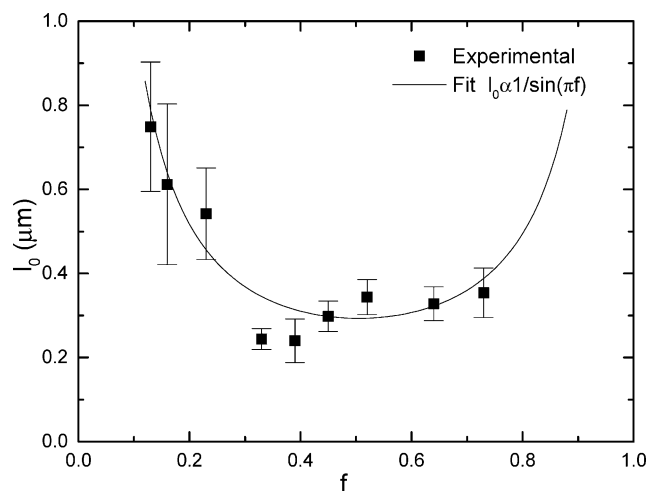


Figure 7. Characteristic length, l_0 , calculated from AFM images, plotted versus coverage, f . Superposed is a best fit using eq 2.

A comparison of the predicted dependence of the characteristic length scale, l_0 , on coverage, f , with experimental measurements, never before reported, provides an additional test of the validity of the physical picture proposed above. This dependence at zero temperature is given by⁴

$$l_0 \propto 1/\sin(\pi f) \quad (2)$$

An appropriate characteristic length has been calculated from the AFM images by determining the mean number of domain boundary intercepts per length of test line. This is plotted versus coverage in Figure 7. Superposed is a best fit using eq 2. The general agreement between the theoretical form and the experimental data is good. It is not possible to guarantee that the observed domain structures are completely equilibrated; however, the patterns were found to be stable (only very slight changes in the contours of some domains were noted) when

resubmerged in pure pentanol for 4 h at both room temperature and 60 °C. The degree of disorder and feature size variation found here at finite temperatures is not surprising when compared with related experimental observations.^{6,13} Finite temperatures and the presence of defects in real experimental conditions lead to significantly greater disorder than expected from the zero temperature simulations. The important point to note is that for these types of systems the equilibrium characteristic length is achieved in relatively short times while orientational order and domain shape refinement continue to evolve over much longer time scales (see, for example, refs 3 and 42). This behavior supports the significance of Figure 7.

The actual value of the characteristic length depends sensitively on the ratio γ_b/γ_d (see eq 1). γ_d is proportional to the product of the dielectric constant of the liquid present during domain formation and the contact potential squared. Contact potential measurements with sufficient spatial resolution can, in principle, be made by electrostatic force microscopy (Kelvin probe force microscopy) and related techniques.⁴³ However, measurements in the presence of a mediating liquid have not been reported and the effect of the liquid on the contact potential (and the interphase boundary energy, γ_b) is not known. Alternatively, electrostatic forces acting on an AFM tip may be measured in solution by force–distance curves.⁴⁴ A very approximate value for the characteristic length can be calculated by setting the sharpness of the interface equal to the measured molecular layer thickness (4.7 nm), the interphase boundary energy to 10^{-12} N (as reported for Langmuir films⁴⁵), the dielectric constant to 13.9 (the value for pentanol⁴⁶), and the contact potential to 0.5 V (in the range reported for alkanethiols on gold⁴⁷). For this set of values $l_0 \sim 100$ nm. To effectively utilize competing interactions to design domain patterns with a controllable length scale, direct measurements of contact potentials and interphase boundary energies for various materials combinations are needed. By manipulating the chemistry of the substrate, solution, and dendrimer (or other) molecules to tailor the electrostatic interactions and interphase boundary energy, domain patterns with repeat distances ranging from a few times the molecular size to microns should be achievable.

Acknowledgment. This work is supported by the MRSEC program of the NSF under Award No. DMR-0213985.

References and Notes

- (1) Andelman, D.; Brochard, F.; Joanny, J.-F. *J. Chem. Phys.* **1987**, *86*, 3673.
- (2) Hurley, M. M.; Singer, S. J. *Phys. Rev. B* **1992**, *46*, 5783.
- (3) Sagui, C.; Desai, R. C. *Phys. Rev. E* **1994**, *49*, 2225.
- (4) Ng, K.-O.; Vanderbilt, D. *Phys. Rev. B* **1995**, *52*, 2177.
- (5) Suo, Z.; Lu, W. *J. Mech. Phys. Solids* **2000**, *48*, 211.
- (6) Seul, M.; Sammon, M. J. *Phys. Rev. Lett.* **1990**, *64*, 1903.
- (7) Seul, M.; Chen, V. S. *Phys. Rev. Lett.* **1993**, *70*, 1658.
- (8) Seul, M.; Andelman, D. *Science* **1995**, *267*, 476.
- (9) McConnell, H. M. *Annu. Rev. Phys. Chem.* **1992**, *42*, 171.
- (10) Allenspach, R.; Stamparoni, M.; Bischof, A. *Phys. Rev. Lett.* **1990**, *65*, 3344.
- (11) Kern, K.; Niehus, H.; Schatz, A.; Zeppenfeld, P.; Goerge, J.; Comsa, G. *Phys. Rev. Lett.* **1991**, *67*, 855.
- (12) Langer, S. A.; Goldstein, R. E.; Jackson, D. P. *Phys. Rev. A* **1992**, *46*, 4894.
- (13) Plass, R.; Last, J. A.; Bartelt, N. C.; Kellogg, G. L. *Nature* **2001**, *412*, 875.
- (14) Tomalia, D. A.; Naylor, A. M.; Goddard, W. A., III. *Angew. Chem.* **1990**, *29*, 138.
- (15) Tomalia, D. A. *Adv. Mater.* **1994**, *6*, 529.
- (16) Grayson, S. M.; Frechet, J. M. J. *Chem. Rev.* **2001**, *101*, 3819.
- (17) Newkome, G. R.; He, E.; Moorefield, C. N. *Chem. Rev.* **1999**, *99*, 1689.
- (18) Zhao, M.; Sun, L.; Crooks, R. M. *J. Am. Chem. Soc.* **1998**, *120*, 4877.
- (19) Balogh, L.; Tomalia, D. A. *J. Am. Chem. Soc.* **1998**, *120*, 7355.
- (20) Zhao, M.; Crooks, R. M. *Adv. Mater.* **1999**, *11*, 217.
- (21) Baker, L. A.; Zamborini, F. P.; Sun, L.; Crooks, R. M. *Anal. Chem.* **1999**, *71*, 4403.
- (22) Rahman, K. M. A.; Durning, C. J.; Turro, N. J.; Tomalia, D. A. *Langmuir* **2000**, *16*, 10154.
- (23) Tokuhisa, H.; Zhao, M.; Baker, L. A.; Phan, V. T.; Dermody, D. L.; Garcia, M. E.; Peez, R. F.; Crooks, R. M.; Mayer, T. T. *J. Am. Chem. Soc.* **1998**, *120*, 4492.
- (24) Zhang, X.; Wilhelm, M.; Klein, J.; Pfaadt, M.; Meijer, E. W. *Langmuir* **2000**, *16*, 3884.
- (25) Street, S. C.; Rar, A.; Zhou, J. N.; Liu, W. J.; Barnard, J. A. *Chem. Mater.* **2001**, *13*, 3669.
- (26) Xu, F. T.; Ye, P. P.; Curry, M.; Barnard, J. A.; Street, S. C. *Trib. Lett.* **2002**, *12*, 189.
- (27) Rar, A.; Curry, M.; Barnard, J. A.; Street, S. C. *Trib. Lett.* **2002**, *12*, 87.
- (28) Coen, M. C.; Lorenz, K.; Kessler, J.; Frey, H.; Mülhaupt, R. *Macromolecules* **1996**, *29*, 8069.
- (29) Sano, M.; Okamuro, J.; Ikeda, A.; Shinkai, S. *Langmuir* **2001**, *17*, 1807.
- (30) Xu, F. T.; Street, S. C.; Barnard, J. A. *Langmuir* **2003**, *19*, 3066.
- (31) Brochard-Wyart, F.; Daillant, J. *Can. J. Phys.* **1990**, *68*, 1084.
- (32) Reiter, G. *Phys. Rev. Lett.* **1992**, *68*, 75.
- (33) Stange, T. G.; Evans, D. F.; Hendrickson, W. A. *Langmuir* **1997**, *13*, 4459.
- (34) Herminghaus, S.; Jacobs, K.; Mecke, K.; Bischof, J.; Fery, A.; Ibn-Elhaj, M.; Schlagowski, S. *Science* **1998**, *282*, 5390.
- (35) Sharma, A.; Jameel, A. T. J. *Colloid Interface Sci.* **1993**, *161*, 190.
- (36) Muller, T.; Yablon, D. G.; Karchner, R.; Knapp, D.; Kleinmar, M. H.; Fang, H.; Durning, C. J.; Tomalia, D. A.; Turro, N. J.; Flynn, G. W. *Langmuir* **2002**, *18*, 7452.
- (37) Li, J.; Piehler, L. T.; Qin, D.; Baker, J. R., Jr.; Tomalia, D. A.; Meier, D. J. *Langmuir* **2000**, *16*, 5613.
- (38) Blizniuk, V. N.; Rinderspacher, F.; Tsukruk, V. V. *Polymer* **1998**, *39*, 5249.
- (39) Tsukruk, V. V.; Rinderspacher, F.; Bliznyuk, V. N. *Langmuir* **1997**, *13*, 2171.
- (40) Voss, R. F.; Laibowitz, R. B.; Alessandrini, E. I. *Phys. Rev. Lett.* **1982**, *49*, 1441.
- (41) Raviv, U.; Laurat, P.; Klein, J. *J. Chem. Phys.* **2002**, *116*, 5167.
- (42) Gao, Y. F.; Sou, Z. *J. Appl. Phys.* **2003**, *93*, 4276.
- (43) Nonnenmacher, M.; O'Boyle, M. P.; Wickramasinghe, H. K. *Appl. Phys. Lett.* **1991**, *58*, 2921.
- (44) Teschke, O.; de Souza, E. F. *Appl. Phys. Lett.* **1999**, *74*, 1755.
- (45) Benvegnu, D. J.; McConnell, H. M. *J. Phys. Chem.* **1992**, *96*, 6820.
- (46) *CRC Handbook of Chemistry and Physics*; Lide, D. R. Ed.; CRC Press: Boca Raton, FL, 1994; p 6-152.
- (47) Evans, S. D.; Ulman, A. *Chem. Phys. Lett.* **1990**, *170*, 462.